

## **REDUCING CONJUNCTION ANALYSIS ERRORS WITH AN ASSIMILATIVE TOOL FOR SATELLITE DRAG SPECIFICATION**

**Geoff Crowley**

Atmospheric & Space Technology Research Associates (ASTRA) LLC  
[gcrowley@astraspace.net](mailto:gcrowley@astraspace.net)

**M. Pilinski**

Atmospheric & Space Technology Research Associates (ASTRA) LLC  
[mpilinski@astraspace.net](mailto:mpilinski@astraspace.net)

### **ABSTRACT**

The upper region of the Earth's atmosphere where the majority of satellites orbit the earth is called the thermosphere. It extends from about 100 km out to about 1500 km. We also refer to the region as 'geospace', but even at these altitudes there is still enough atmospheric gas to affect satellite orbits. We describe the next-generation commercial nowcast and forecast system for specifying the neutral atmospheric state related to orbital drag conditions. This tool, called 'Dragster', is based on several state-of-the-art upper-atmosphere models running in real-time and uses assimilative techniques to produce a thermospheric nowcast. This software will also produce 72 hour predictions of the global satellite-drag conditions using near real-time and predicted space weather data and indices as the inputs. Features of this technique include (1) satellite drag specifications with errors lower than current models; (2) Altitude coverage up to 1000km, (3) Assimilation of satellite drag and other datatypes, (4) Real time capability, (5) Ability to produce 72-hour forecasts of the atmospheric state.

In this paper, we summarize the model design and assimilative architecture, and present preliminary validation results. Validation results will be presented in the context of satellite orbit errors and compared with several leading atmospheric models. As part of the analysis, we compare the drag observed by a variety of 'test' satellites which were not used as part of the assimilation-dataset.

## INTRODUCTION: SATELLITE DRAG AND ORBIT PREDICTION

The upper region of the Earth's atmosphere where the majority of satellites orbit the earth is called the thermosphere. It extends from about 100 km out to about 1500 km. We also refer to the region as 'geospace', but even at these altitudes there is still enough atmospheric gas to affect satellite orbits. Much as aircraft are affected by the prevailing winds and weather conditions in which they fly, satellites are affected by the variability in atmospheric density and the motion of the gas in the near earth space environment, or geospace. Drastic changes in the neutral density of the thermosphere, caused by geomagnetic storms or other phenomena, result in perturbations of LEO satellite motions through atmospheric drag on the satellite surfaces. This can lead to difficulties in locating important satellites, temporarily losing track of satellites, and errors when predicting collisions in space. As the population of satellites in Earth orbit grows, higher space-weather prediction accuracy is required for critical missions, such as accurate catalog maintenance, collision avoidance for manned and unmanned space flight, reentry prediction, satellite lifetime prediction, defining on-board fuel requirements, and satellite attitude dynamics.

Satellite drag varies strongly as a function of the neutral thermospheric density and the satellite ballistic coefficient. Aerodynamic drag acceleration ( $a_{drag}$ ) is expressed by the equation below in terms of atmospheric density ( $\rho$ ), drag coefficient ( $C_D$ ), cross-sectional area ( $A$ ), spacecraft mass ( $m$ ) and the spacecraft velocity relative to the atmosphere ( $V_r$ ).

$$a_{drag} = \frac{1}{2} \rho \frac{C_D A}{m} V_r^2 \quad (1)$$

The drag acceleration is the aerodynamic acceleration projected in the direction of satellite velocity. Many satellites also experience non-negligible lift forces which can cause long-term changes in the orbital inclination as well as aerodynamic torques which can alter the attitude state of the satellite. The inverse ballistic coefficient is often used to describe the non-atmospheric contributions to satellite drag as shown below.

$$B = \frac{C_D A}{m} \quad (2)$$

Thermospheric density is the most variable of these parameters with mass densities ( $\rho$ ) at a constant altitude changing by as much as 200-800% due to changes in geomagnetic activity levels (in other words, during solar storms).<sup>1</sup> Here we define variability as the total change of a parameter divided by the initial value of the parameter. In general, thermospheric density demonstrates variability with latitude, longitude and time due to variable internal forcings, by atmospheric dynamics and waves, and external forcings, by solar EUV flux changes and solar wind disturbances. The product of  $C_D$  and  $A$  is the second contribution to satellite drag variability with variations for elongated satellites flying above 180 km as large as approximately 100%.<sup>2,3</sup> Another 25%-50% change can be expected in the product of  $C_D$  and  $A$  below 180 km due to transition effects.<sup>4,5</sup> Changes in atmospheric winds can lead to changes in  $V_r$  and this can cause changes in satellite drag which are on the order of 3% 1- $\sigma$  with maximum effects on the order of 13% during large geomagnetic storms.<sup>6</sup> Some orbiting objects experience propellant leaks or breakup in which cases changes in mass can cause drag acceleration to be altered by significant amounts (sometimes in excess of 100%) [Bowman and Hrcir 2007] but these cases are beyond the scope of this work.<sup>4</sup>

There are numerous motivations to improve the state of the art modeling of the orbital drag environment. As the population of satellites in Earth orbit grows with time, higher orbital prediction accuracy is required for critical missions, such as accurate catalog maintenance, collision avoidance for manned and unmanned space flight, reentry prediction, satellite lifetime prediction, specifying on-board fuel requirements, and satellite attitude

dynamics. These activities are critical to operational needs in LEO and to Space Situational Awareness efforts. Furthermore, the Committee for the Assessment of NASA's Orbital Debris Programs notes that the ability to maintain a catalogue of space object orbits feeds into NASA and MDA debris and breakup assessment models which support critical needs in hazard detection and risk assessment (“Limiting Future Collision Risk to Spacecraft: An Assessment of NASA’s Meteoroid and Orbital Debris Programs”). This capability for catalogue maintenance, critical to DoD and NASA missions, is complicated by the fact that much of the LEO space object population has orbits which are continuously perturbed by satellite drag.

Thus, improvements in satellite-drag prediction capability are needed and motivate the development of the Dragster system to specify more accurate atmospheric densities. In this paper, we will review the requirements for the Dragster system, present a feasibility study showing the performance of first-principles models as it pertains to satellite-drag operational needs, and review challenges in designing an assimilative space-weather prediction model. Finally, we will present some preliminary modeling results and how they relate to expected orbital errors.

## Dragster MODEL OVERVIEW

Dragster is designed to provide drag specification for the majority of resident space objects (see altitude distribution below) in the region where drag is the most relevant non-conservative orbital perturbation. This region is also populated with critical space assets as seen in the left side of Figure 1. Dragster will specify real-time and forecast densities, compositions, and winds along satellite orbits to compute better drag estimates.

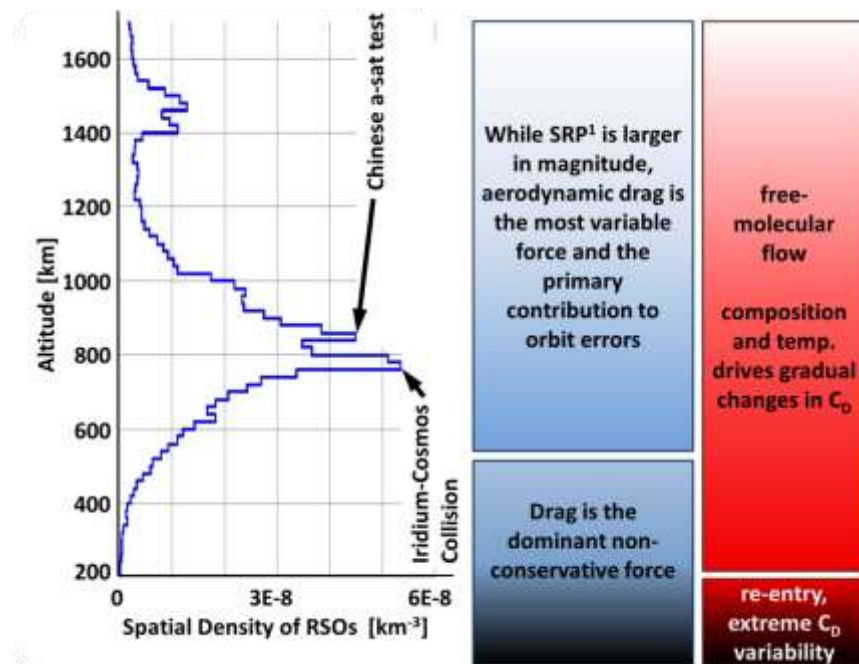


**Figure 1:** Altitude Regions of Relevance to Satellite Drag Specification.

Requirements for the Dragster model nowcast and 3-day forecast are given in the table below. Note that the requirements and goals are based on performance as compared to the leading empirical drag model, Jacchia-Bowman 2008 (JB08), and the leading assimilative empirical model, High Accuracy Satellite Drag Model (HASDM) which is used operationally at the air-force.<sup>7,8</sup> In addition to these requirements, the Dragster software must also run within three hours of real time. This means that the nowcast (and the associated 3-day forecast) is no more

than three hours latent from the time for which it was generated. In order to be used for drag specification, the model must also output self-consistent densities, winds, temperatures, and compositions along an arbitrary satellite orbit.

The JB08 and HASDM models represent the current state of the art for satellite drag prediction and we will now briefly describe them here to provide context for our ongoing work. The JB08 model is an empirical atmospheric density model used operationally by the AF for satellite orbit prediction. It uses state-of-the-art solar indices as well as the Dst geomagnetic index and is finely tuned to match historical satellite drag observations over several solar cycles. JB-08 includes semi-annual variations, some storm response, a low-resolution local-time and latitudinal structure, as well as solar cycle response gleaned from satellite drag observations. The High Accuracy Satellite Drag Model (HASDM) dynamically calibrates a background density model such as JB08 by finding the least squares solution to the model temperature fields at both the “inflection altitude” (~120 km) and the exosphere. Six hour orbit fit-spans from between 70-90 “calibration” satellites are used to determine the spherical expansion of the atmospheric temperature fields. The solved spherical harmonic coefficients and their short-term trends can then be incorporated into an empirical model such as JB08 along with prediction indices to run a 3 day forecast of atmospheric density.

For all their capabilities, the uncertainties in JB08 and HASDM are still too large to satisfy the operational requirements listed in Table 1. In fact, the Air Force Space Command (AFSPC) requirement is neutral density forecasts within 5% over a 72 hour period, something which the present state of the art (HASDM and JB08) do not provide.<sup>9</sup>

**Table 1.** Top Level Dragster Requirements.

	Requirement	Goal
Nowcast	RMSE lower than JB08 more than half the time. <sup>7</sup> <i>JB08: 13-18% at 200-800km</i>	RMSE better than HASDM for storm time. <sup>8</sup> <i>HASDM: 6-8% at 200-800km</i>
72h Forecast	RMSE lower than JB08 in forecast mode	RMSE lower than HASDM in forecast mode

The Dragster model is based on three well-validated Global Circulation Models: (a) the Thermosphere Ionosphere Electrodynamics Global Circulation Model (TIE-GCM), (b) the Thermosphere Ionosphere Mesosphere Electrodynamics Global Circulation Model (TIME-GCM), and (c) the Coupled Thermosphere Ionosphere Plasmasphere electrodynamics (CTIPE). Seminal work by such authors as Mayr et al. [1973] and Dickinson et al. [1981] led to the initial development of a non-linear global thermosphere general circulation model at the National Center for Atmospheric Research (NCAR).<sup>10,11,12</sup> This model evolved over the years with the addition of a self-consistent ionosphere, electrodynamics (TIE-GCM), through to the extension into the mesosphere to become the TIME-GCM.<sup>13,14,15</sup> The TIE-GCM and TIME-GCM can be run at a horizontal resolution of 5°x5° and a vertical resolution of one half pressure scale height ( $H/2$ ).

For satellite drag applications, the global neutral density field is obtained from the thermospheric section of the code. The neutral atmosphere code solves the non-linear momentum, energy, and composition equations time-dependently over the globe, to provide neutral dynamics, temperature, and the distribution of neutral species. The three-dimensional distribution of neutral density is obtained from the temperature and composition, which together with the neutral winds provide the necessary parameters for satellite drag prediction. The self-consistent ionosphere is important and necessary to ensure the accurate conductivities, for characterizing high latitude Joule heating, for ion drag, and for realistic wind determination.

In parallel with the development of the TIE-GCM and TIMEGCM at NCAR, the Coupled Thermosphere Ionosphere Plasmasphere electrodynamics (CTIPe) model followed a similar but independent development cycle. The evolution of CTIPe began with the development of a global thermospheric code, which was later coupled to an ionospheric module, and a plasmasphere and electrodynamics code.<sup>16,17,18</sup> The thermospheric code solves the same set of coupled equations as the NCAR model, but with different resolution, numerical scheme, and time step.

The CTIPe model is a global, three-dimensional, time-dependent, nonlinear, self-consistent model that solves the momentum, energy, and composition equations for the neutral and ionized atmosphere.<sup>19</sup> The global atmosphere in CTIPe is divided into a series of elements in geographic latitude, longitude, and pressure. The latitude resolution is 2°, the longitude resolution is 18°, and each longitude slice sweeps through local time with a 1 min time step. In the vertical direction, the atmosphere is divided into 15 levels in logarithm of pressure from a lower boundary of 1 Pa at 80 km to more than 500 km altitude.

TIE-GCM, TIME-GCM, and CTIPe are used in an assimilative architecture within the Dragster model. Each model type is used to perform ensemble assimilation and hence the various models will sometimes be referred to as super-ensemble members. Dragster will propagate the super-ensemble members forward to predict the most probable trajectory of the thermospheric state and its uncertainty based on inter-model differences. It must be kept in mind that unlike tropospheric weather, the thermosphere is strongly driven by external inputs and depends less on the current and prior states. Therefore, improvements in input forecast will play an important role in reducing satellite drag errors.

## SOFTWARE ARCHITECTURE

The Dragster software modules are outlined by thick boxes in Figure 2. Three boxes represent model drivers: (a) the High-Latitude Forcing Subsystem (light blue); (b) Solar Forcing Subsystem (orange), and; (c) the Lower Boundary Forcing Subsystem (purple). These inputs are used to drive a series of full-physics models in the Super-Ensemble Subsystem (dark blue). The Super-Ensemble Subsystem generates model nowcasts and forecasts out to 72 hours along with estimates of uncertainty. The output model fields are then processed by an Output Processing and Validation Subsystem (grey).

The High Latitude Forcing subsystem (light blue box in upper left of the figure) can specify ionospheric convection patterns through either the Weimer model or AMIE procedure. In the case of Weimer, input data is normally ACE (or DSCOVR) measurements of solar plasma density, plasma velocity, and IMF magnitude and orientation as shown in the right hand side of the light-blue box. Alternatively, a 'correlation module' permits the Weimer convection model to be driven by indices such as Ap, Kp or Dst. The user may also choose to run some or all of the models with AMIE in which case Ground Magnetometer, Ion-Drifts (from DMSP, ISR, and/or SuperDarn) and/or AMPERE data is assimilated to form an optimal solution of the polar cap electrodynamics. The AMIE procedure is described later in the paper. As shown in the left hand side of the light-blue box, the climatology of small scale variability in the high latitude electric field is also specified and passed to the models, as are the particles entering the auroral regions.

In order to forecast satellite drag, density forecasts will be required. These will be driven by model inputs provided by Forecast Modules. A Forecast Module is shown for each of the input subsystems (High Latitude, Solar and Lower Boundary). An instantiation of the Forecast Module in the High-Latitude Forcing Subsystem calls on one of two sources of data as specified by the user. The first option is 72 hour forecasts of Kp and Dst downloaded from their respective servers. The second option is the Enlil Solar Wind Prediction Model which runs in real time and forecasts solar wind plasma density and velocity out to 5 days. The interface between the high latitude inputs and each full-physics model in the super-ensemble is provided by a Unified High Latitude Module (directly below

the light blue box in Figure 2), which is described in more detail below. Enlil forecasts are readily available from both the NOAA SWPC in Boulder, and the CCMC at NASA Goddard.

Solar forcing is specified via the Solar Forcing Subsystem (orange box in the upper right hand corner of the figure). The UV/EUV radiation can be specified through the EUVAC model, which in turn can be driven by any number of operational indices such as M10.7, S10.7, Y10.7, or F10.7. These are also the real-time solar indices being used to drive the JB08 model operationally. Figure 2 shows numerous other options for driving solar forcing; this includes the Solar Irradiance Platform (SIP also known as SOLAR2000PG), SDO/EVE measurements, SRPM model outputs, and FISM model outputs.

An instantiation of the Forecast Module inside the solar forcing subsystem will be able to drive forecasts of most solar input options. Forecasts of the JB08 solar indices can be selected by the user and the SIP, SRPM, and FISM forecasts can also be used in the Dragster system. The solar drivers interface to the models via a Unified Solar Module (directly below the Solar Forcing subsystem), which will provide the solar fluxes in the spectral bands needed to drive each general circulation model in the assimilation module.

Lower boundary forcing (purple box) is divided into two sections specifying eddy diffusion variability near the turbopause ( $K_{zz}$  on the left), and tides (right side of the purple box). Eddy diffusion can be specified climatologically or tuned dynamically. Dynamic tuning of  $K_{zz}$  was successfully implemented in TIME-GCM by Pilinski and Crowley who showed improvements of 5 percentage points in satellite drag specification using this approach.<sup>20</sup> Three choices will be available to the operator when specifying tides: forecast tides (from the Forecast Module), analysis tides, and tidal climatology. A Unified Tide Module standardizes the tidal outputs from these various options into a common format used by all the models (Hough modes). Note that the unified forcing modules (high-latitude, solar, and tidal) each act like an impedance-matching device between each input option and model-type. This ensures that the inputs are compatible with each model and that minimal model-tuning is required when switching input types.

We now turn our attention to the Super-Ensemble Subsystem (dark blue box in the center of Figure 2). Inside this subsystem, three full-physics models are driven by the selected inputs described above. An ensemble of each model-type will be run, consisting of a number ( $N$ ) of members. The number of ensemble members will be user-selectable. Depending on user specifications and model speed, we expect approximately  $N = 20$  to 90 ensemble members will be running for each of the model-types at any given time. The Dragster system described here will employ Ensemble Optimal Interpolation (EnOI) to provide nowcasts of various atmospheric and drag parameters. In the EnOI scheme, data is assimilated into one instantiation of each model type (green boxes in the Super Ensemble Subsystem). The assimilation data is represented by the white boxes labeled "Assimilation Drag Data", and could include accelerometer data, and orbit averaged drag data.

Every three hours, the assimilated states (which include the forcing parameters) are used to initiate three 72 hour forecasts (one for each model type). The nowcast and forecast coming from each model-type is passed out of the Super Ensemble subsystem (green line) as NetCDF files containing density, wind, composition, and temperature fields for each model at the nominal grid resolution. Additional fields (such as electron density) may also be requested by the user. The NetCDF's are passed to an Output Processing and Validation Subsystem (grey box at bottom of the figure).

In the Output Processing and Validation Subsystem, a satellite "Fly-Through" module computes the mass-density, neutral winds, number densities, and temperatures along any specified satellite orbit or series of orbits. These along-orbit parameters are passed to a Ballistic Coefficient and Drag Module, which uses them to compute a physics-based drag coefficient and an estimate of the satellite drag force along the orbit. The Ballistic Module also computes a fitted-ballistic coefficient and examines its multi-year history for any object if a long enough dataset is available. In this way, a long-term average ballistic coefficient, and the best physics-based drag coefficient can be combined to provide a best estimate of satellite area-to-mass ratio to be used in the orbit propagation. The modeled drag force along the satellite orbit is passed to the Validation Module, which uses the information to

compute the energy dissipation rate (EDR) for a collection of validation objects that were not used in the assimilation.<sup>21</sup> The validation data can include accelerometer or orbit-averaged drag measurements. The Validation Module compares the measured and modeled EDR for each object and estimates a series of metrics for the nowcasts and forecasts.

Note that three validation methods are occurring at all times within the Dragster system. The first is an Inherent Validation, which occurs as a result of the assimilation in the Super Ensemble Subsystem. In this validation, assimilation data is compared with the assimilated model state (green box outputs) to compute drag residuals. The second type of validation is the Cross Validation occurring in the Output Processing Subsystem (grey box) for nowcast outputs. The third is the Forecast Validation occurring for the 72-hour forecasts. All three validation metrics are made available to the Decision Module which uses them to combine the assimilated model outputs (NetCDF files) into a single stream of densities, winds, compositions, temperatures, or drag predictions (as desired by the user). The operator chooses whether the Decision Module should apply outlier rejection, simple averaging, weighted-average based on the validation metrics for each model, or simply to choose one model for all times. The result is the best orbit-resolved drag nowcast and 72-h prediction updated every three hours, together with uncertainties in the predictions. This result is passed to an orbit propagator of the user's choosing (external to Dragster).

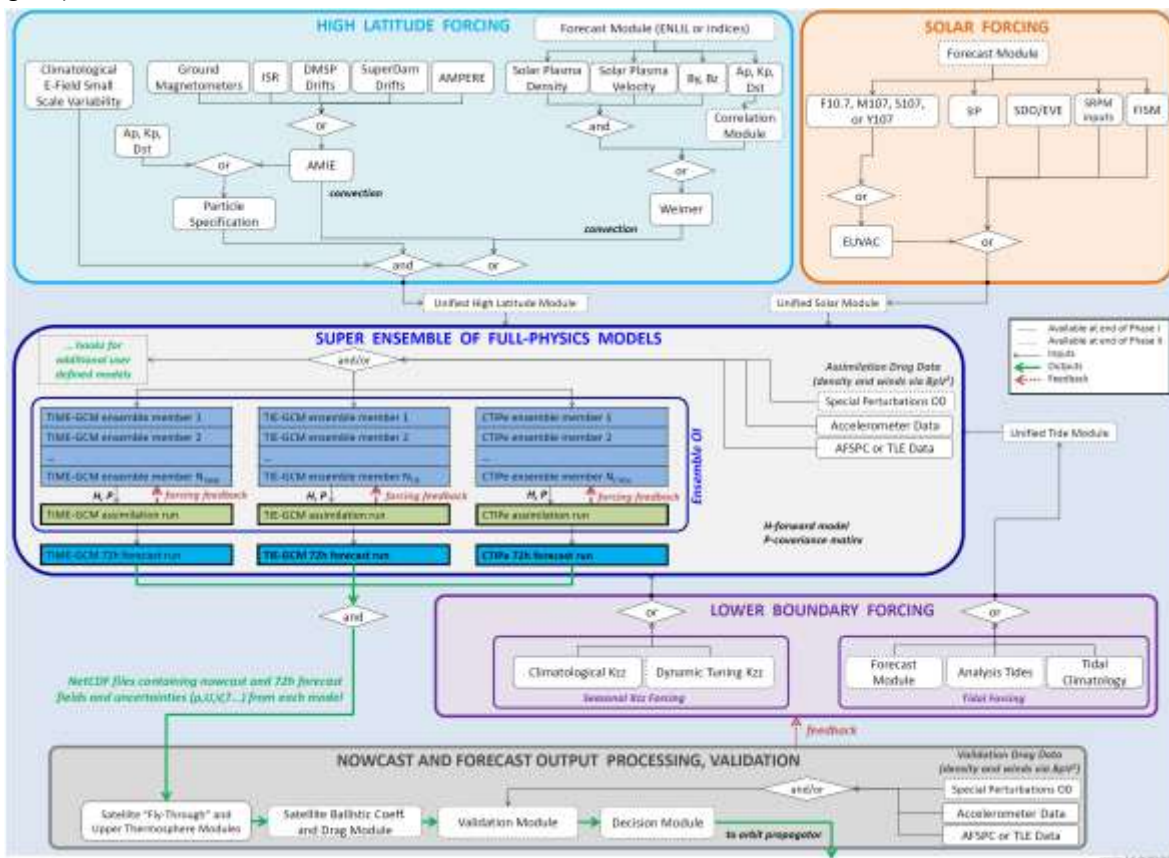


**Figure 2.** A conceptual flow-diagram indicating how the three GCM models may be driven and how the various software modules interact.

## TEST DATA

As mentioned in the previous section, the Dragster model can ingest both accelerometer as well as orbit-averaged drag data. Additional inputs such as composition measurements (from mass spectrometers and imagers) and atmospheric winds will be included as input options in the future. For now, we are testing the model architecture with satellite drag data using two line-elements, daily-averaged densities, and accelerometer data as sources.<sup>22,23,24</sup>

Observation objects were selected according to a set of simple criteria. Selection criteria include a known shape which exhibits little variation in the observed ballistic coefficient and or a stable fitted ballistic coefficient.<sup>25</sup> These criteria allow the ballistic coefficient to be estimated by both apriori means as well as by orbital observation. The goal is to maintain a catalog of 60-80 assimilation/calibration objects and 10-15 validation objects. The validation objects will not be used in assimilation but instead will serve as independent evaluations of assimilation performance. The Dragster object list currently includes 39 assimilation/calibration objects and 10 validation objects which is within our goal. A wide range of inclinations and perigee heights allows Dragster to be sensitive to density changes at all latitudes and altitudes of interest. **Error! Reference source not found.** illustrates a selection of some of the objects in the Dragster catalog along with the altitude and latitude coverage.

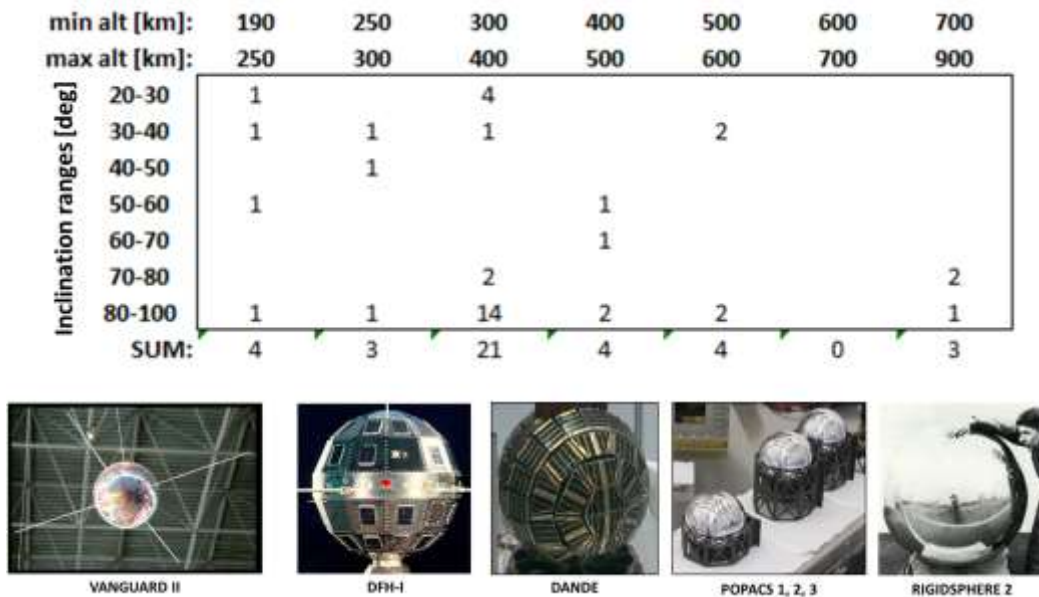


Figure 3: The test dataset for Dragster.

In order to generate data for Dragster assimilation/calibration/validation objects we convert the orbital elements objects into energy dissipation rates (EDR) and effective atmospheric neutral densities. EDR's will be evaluated as the general drag assimilation metric for this project. This is because they can be extended to multiple satellite-drag data sources. Densities and EDR's have been processed for several of the objects in the cal-val table presented in the previous report. This data is used as a stand in for eventual high-task orbital tracking data processed using a special perturbations approach.<sup>22</sup> The TLE dataset is not as accurate as the special perturbation approach. However it is freely available and has very similar sampling properties making it ideal for worst-case testing of our approach. The observed energy dissipation rate between times  $t_i$  and  $t_k$  is generated using the following relationship.

$$\dot{\varepsilon}_{\text{obs}}(t_{ik}) = \frac{\Delta n}{3n_A \mu^{-2/3} \Delta t} \quad (3)$$

where  $\mu$  is the Earth's gravitational parameter,  $\Delta n$  is the change in the mean motion orbital parameter,

$$\Delta n = n(t_k) - n(t_i) \quad (4)$$

$n_A$  is the average mean mean-motion orbital parameter,

$$n_A = (n(t_i) + n(t_k))/2 \quad (5)$$

and  $\Delta t$  is the length of time elapsed

$$\Delta t = t_k - t_i \quad (6)$$

The effective density ascribed to this observation is

$$\rho_{\text{obs}}(t_{ik}) = \frac{2 \cdot \dot{\varepsilon}_{\text{obs}}(t_{ik}) \cdot \Delta t}{B \cdot \int_{t_i}^{t_k} V_{sc}^3 F dt} \quad (7)$$

where  $V_{sc}$  is the spacecraft velocity and  $F$  is the wind factor.<sup>22</sup> Figure 4 shows energy dissipation rates calculated for object 20227 (perigee altitude near 400 km) using TLEs and compared with the special perturbation approach and an expected EDR based on the NRLMSISE-00 model. It demonstrates that the TLE approach approximates the special-perturbations orbital-drag estimates sufficiently well to serve as a test case for assimilation.

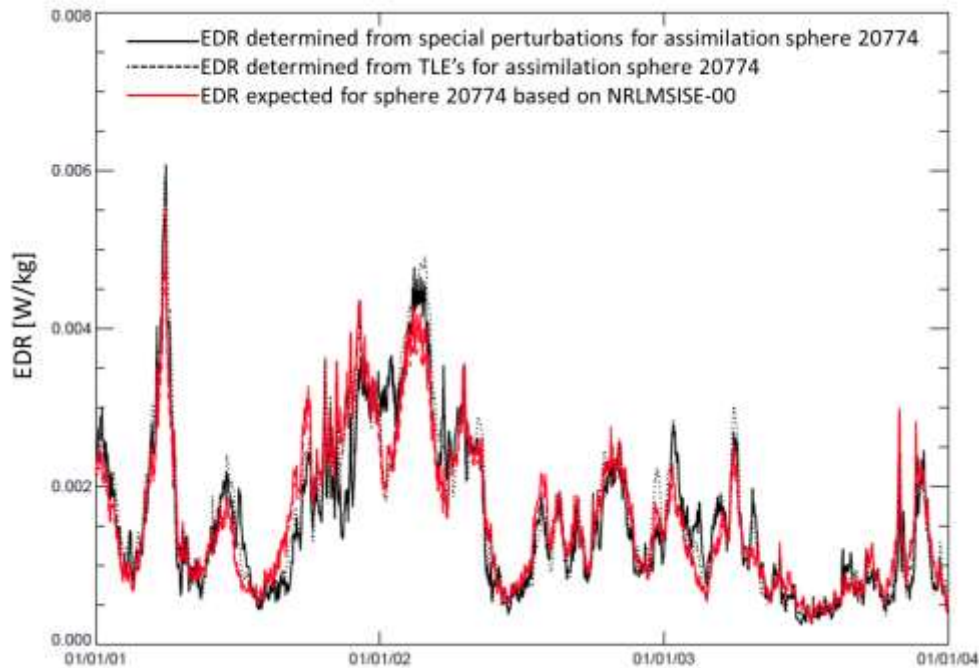


**Figure 4. Energy dissipation rates for NORAD object 20227 near 400 km altitude.**

Figure 5 shows the densities for the DANDE, POPACS-1, POPACS-2, and POPACS-3 assimilation objects with perigee altitudes near 325 km. Note that the objects were launched into the same orbit at the end of 2013 and have not separated significantly over the course of the year plotted in Figure 5. The four objects are shown along

with corresponding effective densities from NRLMSISE-00 empirical model.<sup>26</sup> As expected the effective densities from the four objects track each other reasonably well but deviate from the model quite a lot at times. This indicates that the data contains sufficiently consistent information for providing innovation (difference between the background state and the data) into the assimilation scheme.

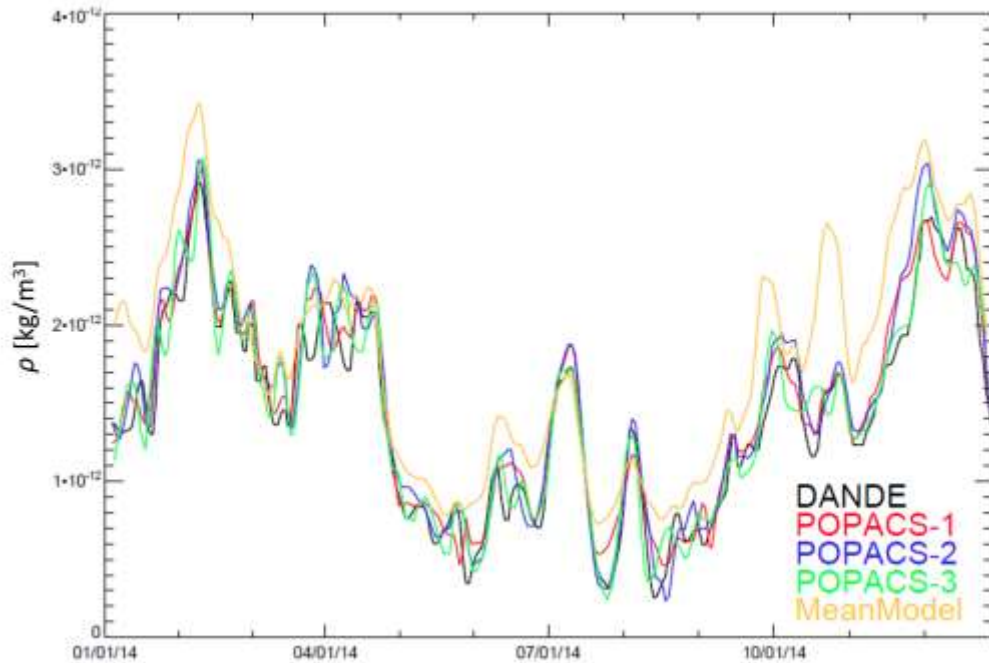


Figure 5. DANDE, POPACS, and NRLMSISE-00 densities near 325 km altitudes.

## DATA ASSIMILATION FOR SPECIFYING GLOBAL SATELLITE DRAG PARAMETERS

Figure 6 shows the Dragster EnKF algorithm flow diagram. The algorithm begins in the upper left with the definition of the initial atmospheric state ( $\mathbf{X}_0$ ) for every ensemble member. The states include a selectable span of model times to accommodate multi-bandwidth datasets. The software propagates all the atmospheric states to the current time and ingests new satellite drag data if it is available. At this point, the ensemble is used to compute the covariance matrices and the Kalman gain. Then, a solution  $\mathbf{X}_a$  is obtained for each ensemble member and the average of these solutions ( $\mathbf{x}_a$ ) is used to initiate a forecast of satellite drag parameters (i.e. densities) to be used for conjunction analysis and orbit prediction. This part of the process is performed iteratively until a pre-specified convergence criterion is met. The iteration and wide time-range incorporated into each state cause this part of the algorithm to resemble a batch processor within an EnKF architecture. This approach along with the inclusion of atmospheric forcings in the state vector has been found to outperform other DA methods when assimilating data into strongly forced systems such as the Earth's upper atmosphere. Dragster then performs a re-sampling of the states based on the current state behavior taking into account the statistical distribution of the forcing parameters. At this point, the algorithm returns to the upper left hand of the flow-diagram and repeats.

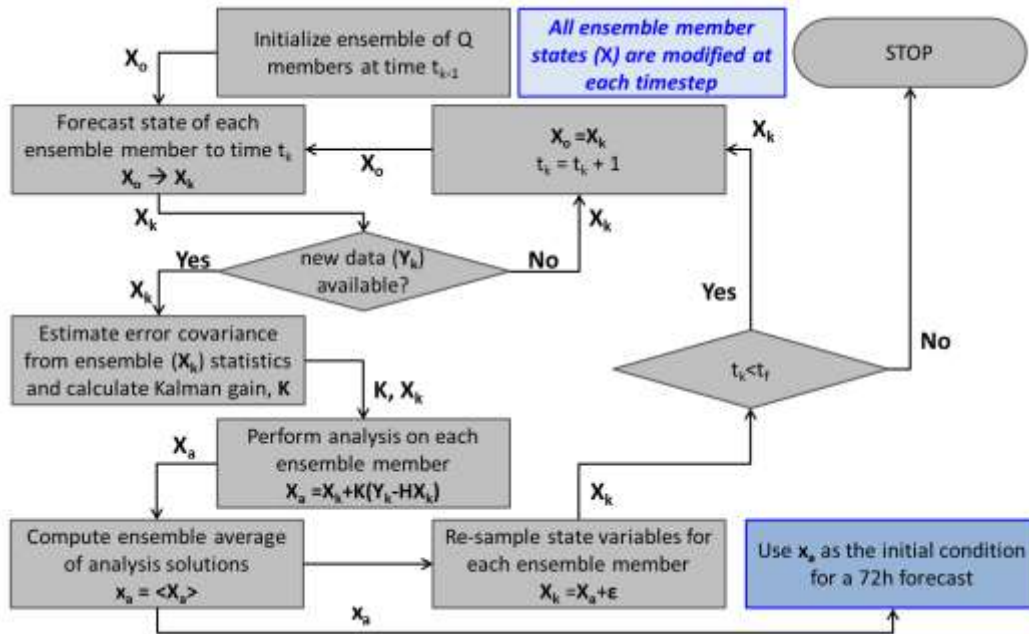


Figure 6: Ensemble Kalman Filter architecture in the Dragster software.

The assimilated state  $x_a$  includes forcing parameters. An instructive test of forcing parameter assimilation is to assimilate synthetic data generated using one model, into an ensemble of that same model. Any resulting discrepancy is due to “process” noise associated with the data bandwidth limitations. In the test case presented below, TLE’s were used as the input data. Figure 7 shows the results of such a test using the Naval Research Laboratory Mass Spectrometer and Incoherent Scatter with Exosphere 2000 model (NRLMSISE-00, sometimes referred to MSIS) as the background. Here, forcing parameters include  $A_p$  (geomagnetic forcing) and F10.7 (solar radiation forcing). The figure shows four time series over the course of four months in 2015. The four time series include measured F10.7 flux (black), F10.7 flux estimated by Dragster (blue), the  $A_p$  planetary geomagnetic index (red), and the  $A_p$  estimated by Dragster (green). Both the F10.7 proxy and  $A_p$  index are plotted on the same y-axis scale. Normal day to day and seasonal variation in solar activity is represented in the plot. A geomagnetic storm in the middle of March is apparent as a sharp peak in the  $A_p$  index. The forcing parameters are recovered quite well in this test and the validation density residuals (density errors for satellites not assimilated into the model) were in the 1-2% range.

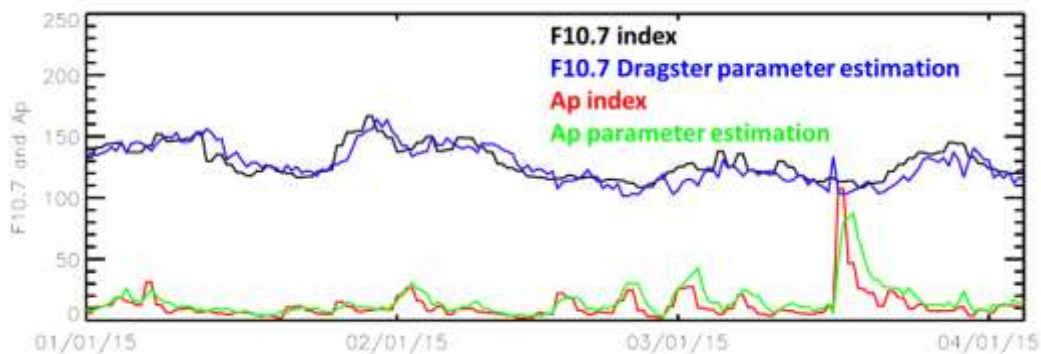
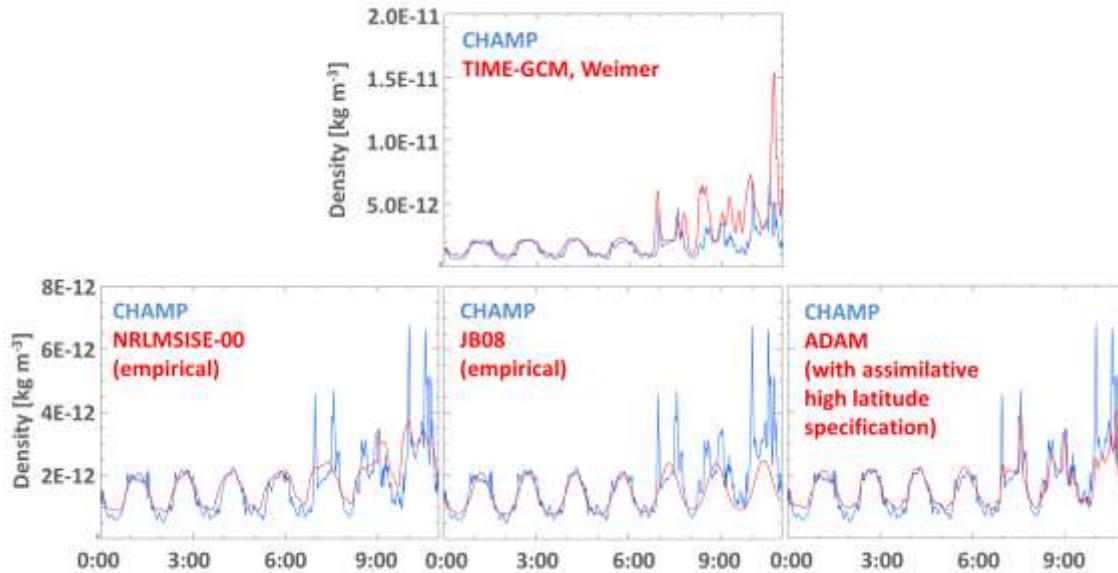


Figure 7: Forcing parameter estimation test using synthetic data and the NRLMSISE-00 model shows the ability to recover atmospheric forcing using imperfect satellite drag data.

## HIGH LATITUDE FORCING SPECIFICATION

Model and measured densities along the CHAMP satellite track during 8/24/2005 geomagnetic storm are shown in Figure 8. Dragster with an assimilative high latitude specification (AMIE in the bottom right panel of the plot) outperforms the empirical models as well as the non-assimilative case (left and center panels in the bottom row of the plot). This shows that the assimilative runs have the potential to vastly improve storm repose modeling and the associated satellite drag specifications when adequate input data is available.



**Figure 8:** Time-series of model and measured densities along the CHAMP satellite track.

## MODEL LOWER BOUNDARY SPECIFICATION

We have tested TIME-GCM dynamic model tuning using feedback from density observations (CHAMP satellite daily-average densities). An a priori density residual is first computed based on the CHAMP measurements

$$\Delta\rho(d) = \frac{\sum_{j=d-40}^{j=d+40} (\rho_j^{\text{obs}} - \rho_j^{\text{mod}})}{\sum_{j=d-40}^{j=d+40} \rho_j^{\text{mod}}} \quad (8)$$

where  $d$  is the day of year,  $\Delta\rho(d)$  is the 81-day density residual centered at  $d$ ,  $\rho_j^{\text{obs}}$  is the daily-average density measured by satellite on day  $j$ , and  $\rho_j^{\text{mod}}$  is the daily-average model density for day  $j$  at the satellite location when the model is run with a constant lower-boundary forcing parameters (Eddy Diffusion coefficient or  $K_{zz}$ ).<sup>20</sup> The lower boundary forcing is then estimated based on a tuning relationship and used to drive the analysis run. The results improve the seasonal signal specification in satellite drag. To evaluate the contribution of lower-boundary

assimilation, the analysis run is compared to a set of validation objects including orbiting Taifun radar calibration spheres and the GRACE-A satellite accelerometer. Densities for the validation of this test were provided by Bruce Bowman at Space Environment Technologies.<sup>23</sup> The table below shows the results of the assimilation. On average, the validation objects indicate a 5 percentage point improvement for the TIME-GCM with lower-boundary assimilation compared to TIME-GCM without assimilation. This technique and results are discussed in more detail by Pilinski and Crowley.<sup>20</sup>

**Table 2:** Daily RMSE for various object-model pairs computed from January 2004 to December 2007 (From Reference 20).

	NRLMSISE-00	TIME-GCM <sup>(1)</sup>	TIME-GCM <sup>(2)</sup>
CHAMP	0.21	0.20	0.15
GRACE-A	0.38	0.23	0.19
#07337	0.21	0.29	0.25
#08744	0.20	0.29	0.24
#12138	0.29	0.29	0.24
#12388	0.19	0.26	0.23
#14483	0.19	0.28	0.23
#20774	0.28	0.30	0.24
<b>average</b>	<b>0.24</b>	<b>0.27</b>	<b>0.22</b>

<sup>(1)</sup>using a constant  $K_{\text{peak}}$ , <sup>(2)</sup>using CHAMP-derived values of  $K_{\text{peak}}$

## ASSIMILATIVE RESULTS

For the preliminary evaluation, drag observations from the orbit data of 75 satellites was assimilated into Dragster using NRLMSISE-00 as the background model. The assimilation spans from January 2015 through December 2015. A 36 hour assimilation window was used with effective-densities spanning the 1.5 day time period advanced forward in time in 0.5 day steps. Dragster solar and geomagnetic forcing parameters as well as density corrections were being estimated using a 90-member ensemble. The spatial resolution for the density corrections was a 15°x15° latitude-longitude grid. Figure 9 below shows the results of the densities from Dragster (gold), HASDM (green), MSIS (red), and JB08 (blue) models for the duration of 2015 compared with TLE-derived densities for the SORCE satellite (~600km altitude). Note that the assimilative Dragster results match very well with the densities experienced by this validation satellite (SORCE was not assimilated into Dragster nor was it assimilated into HASDM). Reproducing the variability seen below depends on accurately representing the seasonal variability in the atmosphere, local-time and latitude structure, response to solar and geomagnetic activity, and implementing an adequate representation of the satellite ballistic coefficients. It is important to note that while HASDM appears to have the largest error, most of this offset is due to a bias between the model and our dataset. A more subtle look at validation errors will follow later in this section.

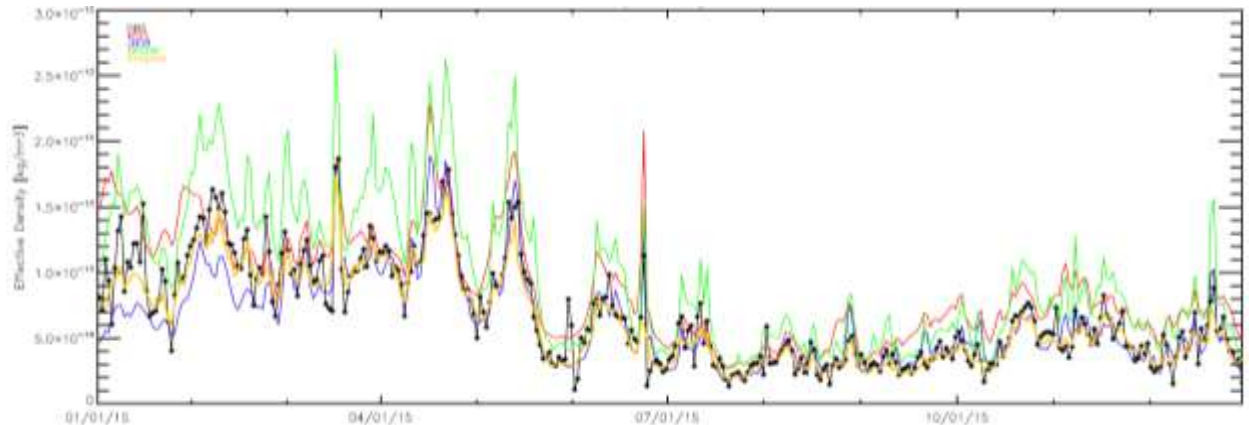


**Figure 9:** One-year time series of observed and modeled densities using the SORCE satellite

We will now use modeled and measured densities based on GRACE satellite accelerometers to evaluate the drag force modeling on the GRACE satellite in an approximately 400 km circular orbit. The equations of motion for both the “truth” or GRACE-density case and the atmospheric-model cases were integrated using a Runge-Kutta 4-5 variable stepsize integrator. The area-to-mass ratio of the representative satellite was taken to be  $0.0027 \text{ m}^2/\text{kg}$  and the drag coefficient was arbitrarily fixed at 3.2. The assumed ballistic coefficient is therefore  $0.0088 \text{ m}^2/\text{kg}$  and will be referred to as  $B^*$ . The drag coefficient is really not fixed along the orbit however it was desired in this case to separate the drag coefficient errors from those caused only by model densities. To further achieve this aim, a “fitted ballistic coefficient” ( $B_{\text{fit}}$ ) was computed during each propagation timespan.

Figure 10 shows a time series of model errors in the early part of 2015 using a 72 hr timespan for orbit propagation. Note that the use of both HASDM and Dragster (assimilative models) result in errors smaller than the orbit propagation performed using the empirical (non-assimilative) MSIS model. A good example of the differences in performance resulting from the use of various atmospheric models is seen just before Day of Year 80 when a geomagnetic storm associated with  $A_p$  values in excess of 100 caused sharp increases in the atmospheric density and in satellite drag. During the storm, 72 hour in track errors exceed 20km when using the MSIS model. However, the in-track errors when using Dragster during this time are 10km. The best performance in this case is achieved by HASDM with approximately 7km in-track errors incurred. It is important to note that the HASDM model in this test used SP orbit solutions which are of much higher cadence and have lower errors than the TLE data ingested into Dragster. We expect Dragster errors to decrease significantly when using such a dataset.

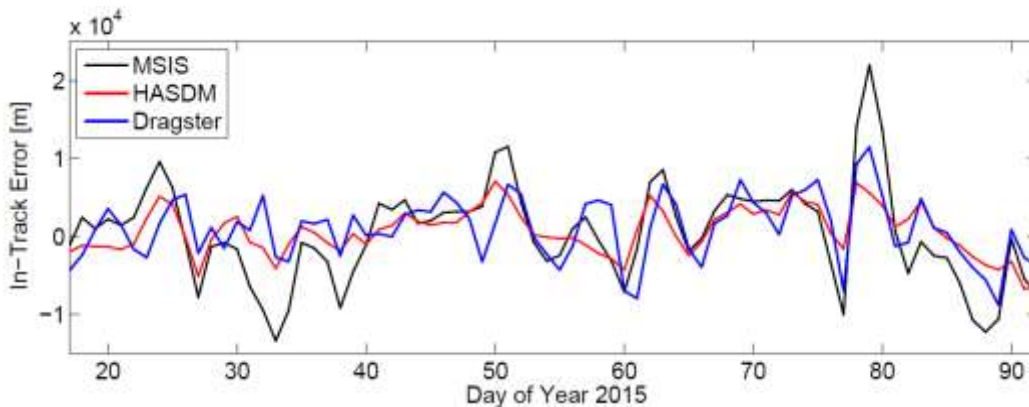


**Figure 10:** 2015 time series of 72-hour in-track errors for the GRACE satellite near 390 km altitude. The larger errors just before Day of Year 80 occur during a strong geomagnetic storm.

These results indicate that the orbit propagation performance (in-track errors) for Dragster is approximately equivalent with that of HASDM (within 5%) in a 72h orbit propagation and that Dragster far outperforms its background model (black line). Recall again that Dragster is driven only by TLE's in this test while HASDM has high cadence observations of satellite orbits. The number of assimilation/calibration objects ingested into both Dragster and HASDM is approximately equivalent but the HASDM operational dataset is much more accurate. We expect that future tests using SP orbit data for all Dragster assimilation objects would result in better performance relative to HASDM. Note also that the Dragster and HASDM standard deviations shown in Table 2 for the GRACE validation satellite were also quite similar (7% vs. 9%) so that similar orbit-propagation statistics are to be expected.

## CONCLUSIONS

A new state-of-the-art assimilative model of the atmosphere called Dragster is being developed at ASTRA in conjunction with its government and academic partners to improve satellite drag specification and forecast. The model incorporates many of the lessons learned from recent research in atmospheric dynamics and assimilation. In particular, the model development takes advantage of the AFOSR-supported Multi-University Research Initiative "Neutral Atmosphere Density Interdisciplinary Research" (NADIR) program. NADIR has laid the groundwork for the development of a first-principles assimilative operational model by deepening our understanding of the basic physical processes that drive the density and winds in the upper atmosphere.

The purpose of the Dragster development is to improve over operational drag-specification below 1000km altitudes in real-time and perform three-day or greater satellite drag forecasts. This altitude range has the advantage of capturing the majority of resident space objects that are affected by changes in the upper atmosphere. The Dragster project's success is evaluated by comparing its performance to empirical atmospheric models as well as the HASDM assimilative model. As we have shown in this paper, Dragster density nowcast performance is already better than that of empirical models even though tests were only run with empirical model background. Furthermore, the Dragster atmospheric density specification is also equivalent to or better than HASDM according to TLE validation analysis. However we point out that these performance gains are limited by the bandwidth of the TLE test dataset. An analysis of orbit propagation performance for the GRACE satellite indicates that in-track orbit errors are equivalent to HASDM near 400km altitudes and improve over the use of NRLMSIS-00 for 3-day and 7-day orbit propagation timespans.

Near-term Dragster test and evaluation efforts are now focused on testing with non-TLE (lower noise) assimilation data and including the first-principles models in the data assimilation scheme. The results of this effort will be reported at next year's event. Interested parties should contact the 1<sup>st</sup> author for more details.

## REFERENCES

- 
- <sup>1</sup> Bruinsma, S. L., and J. M. Forbes (2007), Storm-Time Equatorial Density Enhancements Observed by CHAMP and GRACE, *J. Spacecraft and Rockets*, Vol. 44, No. 6, doi: 10.2514/1.28134.
- <sup>2</sup> Doornbos E. (2011). Thermospheric Density and Wind Determination from Satellite Dynamics. PhD thesis, Delft University of Technology.
- <sup>3</sup> Pilinski, M. D. and B. Argrow (2013a), Aerodynamic analysis based on CHAMP satellite lift-to-drag measurements, *J. Spacecraft and Rockets*, doi: 10.2514/1.A32394.
- <sup>4</sup> Bowman B. R. and S. Hrnrcir (2007). Drag Coefficient Variability at 100-300 km from the Orbit Decay Analyses of Rocket Bodies. In AAS/AIAA Astrodynamics Specialist Conference, number AAS 07-262. AAS/AIAA.
- <sup>5</sup> Pilinski M. D., B. M. Argrow, S. E. Palo, B. R. Bowman (2013b), Semi-Empirical Satellite Accommodation Model for Spherical and Randomly Tumbling Objects, *Journal of Spacecraft and Rockets*, Vol. 50, pp. 556-571, doi: 10.2514/1.A32348 .
- <sup>6</sup> Crowley, G., Pilinski, M., and Azeem, I. (2012), Tutorial: The Neutral Atmosphere and the Satellite Drag Environment, AAS 12-035, 145-161.
- <sup>7</sup> Bowman, B. R., W. K. Tobiska, F. A. Marcos, C. Y. Huang, C. S. Lin, and W. J. Burke (2008b), A new empirical thermospheric density model JB2008 using new solar and geomagnetic indices, paper presented at the AIAA/AAS Astrodynamics Specialist Conference, Am. Inst. of Aeron. and Astron., Honolulu, Hawaii, 18–21 Aug 2008.
- <sup>8</sup> Storz, M., B. R. Bowman, J. I. Branson, and S. J. Casali (2005), “High accuracy satellite drag model (HASDM)”, *Advances in Space Research*, Vol. 36, pp. 2497–2505.
- <sup>9</sup> Marcos, F. A., S. T. Lai, C. Y. Huang, C. S. Lin, J. M. Retterer, S. H. Delay, and E. Sutton (2010), Towards Next Level Satellite Drag Modeling. In Atmospheric and Space Environments Conference, number 2010-7840. AIAA.
- <sup>10</sup> Mayr, H. G. and H. Volland (1973), Magnetic storm characteristics of the thermosphere, *J. Geophys. Res.*, 78(13), 2251–2264, doi:10.1029/JA078i013p02251.
- <sup>11</sup> Dickinson, R. E., E. C. Ridley, and R. G. Roble (1981), A three-dimensional general circulation model of the thermosphere, *J. Geophys. Res.*, 86, 1499– 1512.
- <sup>12</sup> Roble, R. G., Dickinson, R. E. and Ridley, E. C. (1982) Global circulation and temperature structure of the thermosphere with high-latitude plasma convection. *J. Geophys. Res.* 81, p. 1599.
- <sup>13</sup> Roble, R.G., Emery, B.A. and Ridley, E.C. (1986). Ionospheric and thermospheric response over Millstone Hill to the May 30, 1984, annular solar eclipse. *Journal of Geophysical Research*, 91(A2): doi: 10.1029/JGREA0000910000A2001661000001. issn: 0148-0227.
- <sup>14</sup> Richmond, A. D., E. C. Ridley, and R. G. Roble (1992), A thermosphere/ionosphere general circulation model with coupled electrodynamics, *Geophys. Res. Lett.*, 19, p. 601.
- <sup>15</sup> Roble, R. G., and E. C. Ridley (1994), A thermosphere-ionosphere-mesosphere electrodynamics general circulation model (TIME GCM): Equinox solar cycle minimum simulations (30– 500 km), *Geophys. Res. Lett.*, 21, 417–420.
- <sup>16</sup> Fuller-Rowell, T. J., Rees, D., Quegan, S., Moffett, R. J., Codrescu, M. V., and Millward, G. H. (1996), A coupled thermosphere-ionosphere model (CTIM), in *Handbook of Ionospheric Models*, edited by R. W. Schunk, Utah State Univ., Logan, Utah, 217–238.
- <sup>17</sup> Fuller-Rowell, T. J. (1984), A two-dimensional, high-resolution, nested-grid model of the thermosphere: 1. Neutral response to an electric field “spike”, *J. Geophys. Res.*, 89(A5),2971–2990, doi:10.1029/JA089iA05p02971.
- <sup>18</sup> Millward, G. H., H. Rishbeth, T. J. Fuller-Rowell, A. D. Aylward, S. Quegan, and R. J. Moffett (1996), Ionospheric F2 later seasonal and semiannual variations, *J. Geophys. Res.*, 101, 5149–5156, doi:10.1029/95JA03343.
- <sup>19</sup> Millward, G. H., I. C. F. Müller-Wodarg, A. D. Aylward, T. J. Fuller-Rowell, A. D. Richmond, and R. J. Moffett (2001), An investigation into the influence of tidal forcing on F region equatorial vertical ion drift using a global ionosphere-thermosphere model with coupled electrodynamics, *J. Geophys. Res.*, 106, 24733-24744.
- <sup>20</sup> Pilinski, M. D., and G. Crowley (2015), Seasonal variability in global eddy diffusion and the effect on neutral density. *J. Geophys. Res. Space Physics*, 120, 3097–3117, doi: 10.1002/2015JA021084.

<sup>21</sup> Storz, M. F. (1999), Satellite Drag Accuracy Improvements Estimated from Orbital Energy Dissipation Rates. *Advances in the Astronautical Sciences*, (99-385).

<sup>22</sup> Picone, J. M., J. T. Emmert, and J. L. Lean (2002). Thermospheric densities derived from spacecraft orbits: Accurate processing of two-line element sets. *Journal of Geophysical Research*, 110(A03301).

<sup>23</sup> Bowman B. R., F. A. Marcos, M. J. Kendra (2004), A Method for Computing Accurate Daily Atmospheric Density Values from Satellite Drag Data, AAS 2004-173, AAS/AIAA Spaceflight Mechanics Meeting, Maui, HI, February.

<sup>24</sup> Sutton, E. K., R. S. Nerem, and J. M. Forbes (2007), Density and winds in the thermosphere deduced from accelerometer data, *J. Spacecraft and Rockets*, 44(6), 1210, doi:10.2514/1.28641.

<sup>25</sup> Bowman, B. R., "True Satellite Ballistic Coefficient Determination for HASDM," AIAA/American Astronautical Society Astrodynamics Specialist Conference and Exhibit, Monterey, CA, 2002

<sup>26</sup> Picone, J. M., Hedin, A. E., and Drob, D. P., "NRLMSISE-00 Empirical Model of the Atmosphere: Statistical Comparisons and Scientific Issues," *Journal of Geophysical Research*, Vol. 107, No. A12, 2002, Paper 1468. doi:10.1029/2002JA009430